PCCP

Accepted Manuscript

This article can be cited before page numbers have been issued, to do this please use: L. Andjelkovic, S. Stepanovic, F. Vlahovic, M. Zlatar and M. Gruden, *Phys. Chem. Chem. Phys.*, 2016, DOI: 10.1039/C6CP03859J.

ROYAL SOCIETY OF CHEMISTRY

www.rsc.org/pccp

View Article Online
DOI: 10.1039/C6CP03859J

Journal Name

ARTICLE

Resolving origin of the multimode Jahn-Teller effect in metallophthalocyanines

Lj. Andjelković[a], S. Stepanović[a], F. Vlahović[b], M. Zlatar[a], M. Gruden[c,*]

Received 00th January 20xx,
Accepted 00th January 20xx

DOI: 10.1039/x0xx00000x

www.rsc.org/

A detailed Density Functional Theory (DFT) analysis was performed in order to study the multimode Jahn-Teller (JT) problem in the electronic ground state of manganese phthalocyanine (MnPc). Comparison with magnesium phthalocyanine ion ($MgPc^-$) and phthalocyanine trianion (Pc^{3-}), also prone to the JT effect, is presented. Our results clarify the origin and provide the microscopic insight into the symmetry breaking process. The JT distortion is highly influenced by the coordination of phthalocyanine to the Mn^{II} ion, and occurs over the whole system, while $MgPc^-$ complex ion possesses mainly ligand-based instability.

Introduction

Phthalocyanines, structurally close to biologically relevant porphyrins, are molecules of the utmost importance in nanoelectronics,[1] optoelectronics,[2] chemical sensors,[3] and so forth. Although the first phthalocyanine was synthesized more than a century ago,[4] the development of new functional phthalocyanines is still relentlessly growing, due to their unique properties[5] and various potential uses in the modern science. Coordination to a metal ion leads to a great diversity of possibilities in the technological application, *e.g.* they are richly utilized as dyes[6] and catalysts[7]. Profound investigations indicate that atomically thin films of transition metal (TM) (copper, nickel, cobalt, iron, manganese) phthalocyanines, initially insulators, can become conductors through potassium doping, opening the way to a new class of superconductors.[8,9] Manganese phthalocyanine (MnPc) belongs to the class of organic semiconductors and molecular magnets.[10] MnPc acts as a spin-filter and its spin can be controlled in the defined manner,[11-14] presenting an important prerequisite for the possible use in molecular spintronics and quantum computing.[15-18] Therefore, metallophthalocyanines are deservedly called "the compounds of the 2lst century".[19] Many ideas, questions and concerns related to the practical applications of this class of compounds require a quantitative understanding of the chemistry and physics on the microscopic level.

Since 3d TM ion complexes in different spin states usually display quite different structural, spectral and magnetic properties, and also reactivity, it is important to correctly determine the spin ground state of the system. For instance, Mn^{II} in MnPc has five d-electrons that can be distributed in a square-planar environment in three different ways: with a maximum number of unpaired electrons, leading to the high spin state, with maximally paired electrons – resulting in the low spin state, or intermediate spin. It was found that intermediate spin is the ground state,[20] however, different ground electronic states within this spin multiplicity are still a subject of debate in the literature.[21-27] In order to clarify these issues we performed Density Functional Theory (DFT) calculations with various Density Functional Approximations (DFAs) reliable for the spin state energetics. Furthermore, one of the possible, already reported, lowest-lying states, ^4E_g, is the subject to the Jahn-Teller (JT) distortion.[28,29] To the best of our knowledge, the JT effect in MnPc was not analyzed so far, even the significance of the JT distortion and its influence on the properties of the systems is well recognized.[29] The distortion can be the inherent feature of the central metal ion in TM compounds, but may also originate from the ligand itself. Therefore, the comparison between 3s-metallophthalocyanine, magnesium phthalocyanine ion ($MgPc^-$), and 3d-metallophthalocyanine, MnPc, can give answers on the nature of the distortion. Furthermore, the question is what happens with phthalocyanine trianion (Pc^{3-}) that itself is an example of multimode $E\otimes(b_1+b_2)$ JT problem, the same as aforementioned complexes. For this purpose we performed DFT approach, developed by Daul at al.,[30,31] proven to be accurate for the analysis of the JT effect in medium-to-large molecules.[32-36] In addition, energy decomposition analysis

[a] Department of Chemistry, IChTM, University of Belgrade, Studentski Trg 12-16, 11001 Belgrade, Republic of Serbia
[b] Innovation center of the Faculty of Chemistry, University of Belgrade, Studentski Trg 12-16, 11001 Belgrade, Republic of Serbia
[c] Center for Computational Chemistry and Bioinformatics, Faculty of Chemistry, University of Belgrade, Studentski Trg 12-16, 11001 Belgrade, Republic of Serbia

(EDA),[37] the powerful tool for generating a compact, qualitative and quantitative picture of a chemical bond formation between the ligand and central metal ion,[38] was performed to afford microscopic insight into the macroscopic features. In this way we can explore different energy contributions and provide information about the changes that occur after the chemical bond is formed enabling us to understand how the central metal ion influences the distortion in these molecules, and hence how electronic structure control the nuclear motion in similar systems. In order to tackle the multimode problem and quantify the role played by different normal modes in symmetry breaking processes, the Intrinsic Distortion Path (IDP) model is employed.[31-33,39,40] The essence of the IDP model is to analyze multimode JT effect within harmonic approximation and to provide important chemical information like an approximation to the minimum energy path, and quantification of the forces along each JT active mode, or in other words calculation of the vibronic coupling constants.

Computational details

The DFT calculations have been carried out using the Amsterdam Density Functional program package, ADF2013.01.[41-43] Geometry optimizations of Pc^{3-}, $MgPc^{-}$ and MnPc was performed using local density approximation (LDA) characterized by the Vosko-Willk-Nusair (VWN) parameterization,[44] as well as with general gradient approximation (GGA) in the form of OPBE[45] and with hybrid B3LYP*[46] functional. Molecular orbitals were expanded in an uncontracted set of Slater type orbitals (STOs) of Triple-zeta quality with double polarization function (TZ2P) basis set.[47,48] All electrons were treated explicitly during the geometry optimizations. An auxiliary set of s, p, d, f, and g STOs was used to fit the molecular density and to represent the Coulomb and exchange potentials accurately for each SCF cycle. All calculations were spin-unrestricted. Geometries of all possible spin states (doublet, quartet and sextet) of MnPc were fully optimized. In addition, by imposing different occupation in the Kohn-Sham (KS) MOs, three intermediate spin states (^4E_g, $^4A_{2g}$, $^4B_{2g}$) of MnPC are considered. For this purpose, energies and gradients were calculated also using BP86-D3,[49-51] S12g,[52] SSB-D,[52] M06-L,[53] PBE0[54,55] and TPSSh[56] DFAs. For all calculations Becke grid of normal quality was used.[57,58] Harmonic frequencies were calculated in order to ascertain that all optimized structures are stationary points on the potential energy surfaces.

In order to quantify the JT effect in the cases where the ground state is orbitally degenerate, geometries and energies of the high symmetry (HS), D_{4h}, and low symmetry (LS), D_{2h}, nuclear arrangements should be known. The multideterminant electronic state of the HS configuration is represented with the average of configuration (AOC) SCF calculation,[30] where the degenerate orbitals are equally populated, leading to a homogenous distribution of electrons over the components of the degenerate irreducible representations (irrep). The AOC approach gives a proper geometry of the HS species. In order to get the energy of the HS molecular configuration, a single point calculation imposing the lower symmetry of the electron density is performed (second step). The last, straightforward step involves geometry optimization of the LS structures, yielding different LS geometries depending on the particular occupation of the originally degenerate KS MOs. The lowest energy structure is the minimum, while other LS structure is the saddle point. Their energy difference is the warping barrier, Δ. The JT stabilization energy (E_{JT}) is the difference in energies obtained in the second and the last step for the structures with the same electron distribution. The JT radius (R_{JT}), describing a direction and magnitude of the JT distortion, is given by the length of the distortion vector between the HS and the LS minimum energy configurations.

The nature of metal-ligand bonding in $MgPc^{-}$ and MnPc was analyzed with the aid of the EDA method[59,60] as implemented in ADF.[42,43] The interaction energy, E_{int}, between two fragments is decomposed into electrostatic, Pauli repulsion, and orbital interaction terms. The first term is the quasi-classical electrostatic interaction between the fragments; the second term is the repulsive Pauli interaction between occupied orbitals on the two fragments; the last term is the stabilizing interaction between the occupied MOs from one fragment with the unoccupied MOs of the other fragment and polarization in the same fragment. In attempt to clarify the origin of the JT distortion EDA was performed on the HS, as well as, on the LS distorted structures. In order to get E_{JT}, in addition to the changes in E_{int} when breaking the symmetry, it is necessary to consider changes in the preparation energies of the fragments, ΔE_{prep} as well:

$$-E_{\mathrm{JT}} = \left(E_{int}(\mathrm{LS}) - E_{int}(\mathrm{HS})\right) + \left(E_{prep}(\mathrm{LS}) - E_{prep}(\mathrm{HS})\right) = \Delta E_{int} + \Delta E_{prep} \qquad (1)$$

View Article Online
DOI: 10.1039/C6CP03859J

The IDP, [31-33,39,40] method for the analysis of the multimode JT problem, is based on the fact that all the information about the vibronic coupling at the HS nuclear arrangement is also contained in the distorted LS minimum energy structure. The reference point for the method is the LS configuration, a true minimum on the potential energy surface, and the distortion is given as a superposition of all totally symmetric normal modes in the LS point group. The IDP is a reaction path starting from the HS geometry and ending in the LS minimum using the quadratic energy surface:

$$E_{\mathrm{JT}} = \sum_i \frac{1}{2} K_i^{LS} \left[\vec{Q}_i^{LS}(HS)\right]^2 \qquad (2)$$

where $\vec{Q}_i^{LS}(HS)$ is the HS geometry expressed in terms of the LS vibrational modes, and K_i^{LS} are the harmonic force constants of the LS normal modes obtained from the DFT calculations. With this model it is possible to directly distinguish the contributions of the different normal modes to the JT distortion, the forces along either LS or HS normal modes at the HS point, as well as how these forces change along a relevant particular path of distortion. $\vec{R}_{JT}$ is expressed in terms of either LS or HS normal modes:

$$\vec{R}_{\mathrm{JT}} = \sum_i r_{JT,i}^{LS} \vec{Q}_i^{LS} = \sum_i r_{JT,i}^{HS} \vec{Q}_i^{HS} \qquad (3)$$

where $r_{JT,i}$ is the contribution of the displacements along the LS or HS normal coordinate to the $\vec{R}_{\mathrm{JT}}$, or in other words the JT radius of the particular normal mode.

Results and Discussion

In order to clarify the complicated electronic structure of MnPc, DFT calculations for its lowest lying electronic states were performed using various DFAs. Mn^{II} in the square-planar environment has five electrons in the 3d shell, leading to the three possible spin states: low spin, S=1/2, intermediate spin, S=3/2 and high spin, S=5/2. These three spin states produce five lowest lying electronic states, out of which three belong to the intermediate spin state, Table 1 and Figure 1. Other possible electronic states are at least 20 kcal mol^{-1} higher in energy than the high spin state, and thus, is excluded from further consideration. Although previous experimental[21-24,61] and theoretical studies[22,25,62-64] have agreed that intermediate spin state is the ground state, the order of the close-lying quartet electronic states is still not clear. According to the different experimental techniques, the ground state is either assigned as ^4E_g,[23,26,62-64] or ^4E_g and $^4A_{2g}$ are equally possible[21,22]. Single-crystal magnetic study found $^4A_{2g}$ as the electronic ground state.[27] Previous experimental study[65] revealed $^4A_{2g}$ ground state into which the excited ^4E_g term is mixed by spin–orbit coupling. Our DFT calculations revealed that regardless of the DFAs used, intermediate spin (1 on the Figure 1), ^4E_g, is the ground state, Table 1.

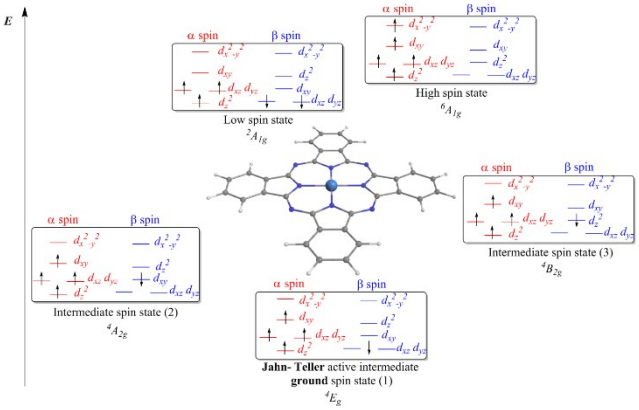

Figure 1. Qualitative energetics and electronic configurations for the five lowest lying electronic states of MnPc calculated with B3LYP*.

It is worth to mention that GGAs and meta-GGA gave that ^4E_g is more stable than $^4A_{2g}$ (depicted in the Figure 1 as 2), and $^4B_{2g}$ (3 on the Figure 1) for approximately 10 kcal mol^{-1}. In the case of OPBE, a large energy difference between intermediate spin $^4B_{2g}$ and $^4A_{2g}$ states is obtained. The energy difference between ^4E_g and $^4A_{2g}$ calculated with hybrids, B3LYP*, PBE0 and TPSSh, is smaller, Table 1. It is well-known fact that some GGAs such as OPBE, S12g and SSB-D, as well as M06-L, B3LYP* and TPSSh are superior for the determination of energy difference between various spin states,[46,66-70] but since the three lowest electronic states belong to the same intermediate spin state, it should not be surprising that hybrid functionals perform better. B3LYP* and TPSSh gave good relative spin state energetics, while PBE0 artificially stabilized the high spin state.

In summary, irrespective of the choice of DFAs ^4E_g is the ground state. This degenerate electronic ground state is prone to the JT distortion, same as in the case of $MgPc^-$ and Pc^{3-}. All three considered molecules in the electronic ground state have a single electron or a hole in a doubly degenerate HOMO, leading to ^2E_g (^4E_g for MnPc) ground electronic state, in perfect square-planar nuclear configurations that belong to the D_{4h} point group. The symmetric direct product of the E_g electronic state transforms as $A_{1g}+B_{1g}+B_{2g}$, giving the symmetries of the JT active normal modes. These three vibrations in square-planar structures are depicted in Figure 2, using the vibrational energy distribution representation.[71]

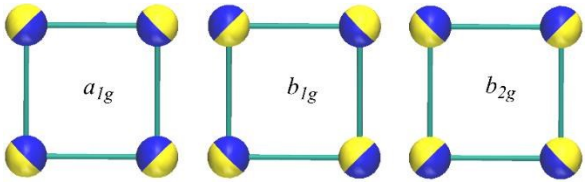

Figure 2. Schematic vibrational energy distribution representation of the a_{1g}, b_{1g} and b_{2g} normal modes in D_{4h} point group. The different colors indicate the direction of the displacement vector.

View Article Online
DOI: 10.1039/C6CP03859J

Table 1. Energy differences (kcal mol^{-1}) for the five lowest lying electronic states of MnPc calculated with different DFAs.

Electronic state		BP86-D3	OPBE	S12g	SSB-	M06-	B3LYP*	PBE0	TPSSh
Low spin	$^2A_{1g}$	24.25	17.4	17.3	32.49	16.51	16.92	22.4	15.76
Intermediate spin (1)	^4E_g	0.00	0.00	0.00	0.00	0.00	0.00	0.00	0.00
Intermediate spin (2)	$^4A_{2g}$	8.81	11.2	12.2	12.41	15.35	3.97	2.63	5.45
Intermediate spin (3)	$^4B_{2g}$	10.79	17.2	12.1	12.78	13.15	6.94	7.75	8.67
High spin	$^6A_{1g}$	25.20	15.4	19.9	14.66	12.94	13.31	4.59	16.33

Vibrations that belong to both B_{1g} and B_{2g} irreps in D_{4h} point group distort square-planar structure to a structure with lower D_{2h} symmetry, rhombus and rectangle, respectively. In the case of investigated molecules, the distortion is not obvious as in the simple JT active square-planar molecules because of a delocalized nature of the active normal modes, but it primarily occurs in the square labeled in Figure 3. Our calculations revealed that in all three cases, b_{1g} normal modes in D_{4h} point group lead to the minima, while b_{2g} ones guide the molecules to the transition states on the potential energy surfaces. As a consequence, ^2E_g (^4E_g) ground electronic state splits into two non-degenerate electronic states, $^2B_{3g}$ ($^4B_{3g}$) and $^2B_{2g}$ ($^4B_{2g}$) in D_{2h} point group, resulting in the stabilization of the molecules.

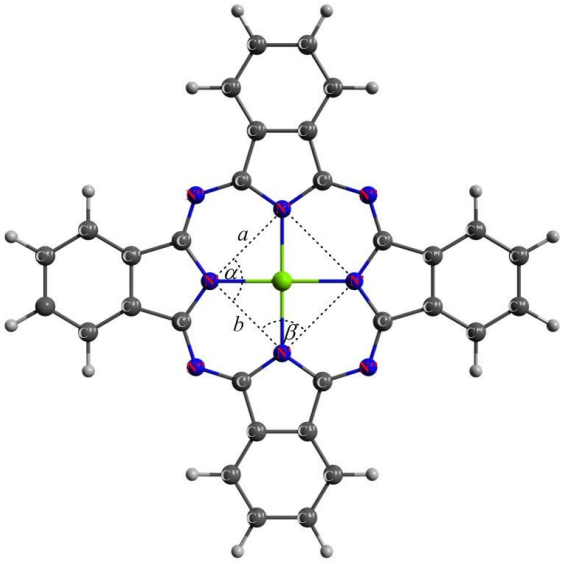

Figure 3. Schematic representation of the LS structures in investigated molecules. Nitrogen and carbon atoms are labelled as N′, C′, N″ and C″.

The JT parameters, E_{JT}, Δ and R_{JT}, for Pc^{3-}, $MgPc^-$ and MnPc were calculated by well-established DFT procedure[30-36] with LDA, OPBE and B3LYP*, Table 2. The choice of DFA have been made from previous experience in determination of the JT parameters by DFT,[30-36] where LDA is shown to be the most accurate functional in comparison with other theoretical and/or experimental results. In this work obtained values do not depend significantly on a choice of DFAs, except in the case of B3LYP* where somewhat higher values of the JT parameters were noticed for Pc^{3-} and $MgPc^-$, Table 2. Insertion of Mg^{II} in the phthalocyanine core leads to the higher JT stabilization energies, although overall distortion is smaller, Table 2. According to earlier DFT study,[72] the values of E_{JT} for minimum and transition state of $MgPc^-$ were 406 and 187 cm^{-1}, respectively, which is in very good agreement with our calculations, although the computation procedures differ.

Table 2. Results of the DFT calculations performed to analyze the JT effect in Pc^{3-}, $MgPc^-$ and MnPc; the JT parameters E_{JT} and Δ are given in cm^{-1} and R_{JT} in (amu)$^{1/2}$Å.

Molecule	Symmetry	LDA	OPBE	B3LYP*
Pc^{3-}	E_{JT}, $^2B_{2g}$	319	331	454
	E_{JT}, $^2B_{3g}$	141	146	253
	E_{JT} (IDP), $^2B_{2g}$	305	311	465
	E_{JT} (IDP), $^2B_{3g}$	142	148	214
	Δ	178	185	201
	R_{JT}, $^2B_{2g}$	0.34	0.32	0.34
	R_{JT}, $^2B_{3g}$	0.21	0.26	0.20
$MgPc^-$	E_{JT}, $^2B_{2g}$	399	421	614
	E_{JT}, $^2B_{3g}$	181	194	273
	E_{JT} (IDP), $^2B_{2g}$	402	417	606
	E_{JT} (IDP), $^2B_{3g}$	191	204	277
	Δ	218	227	341
	R_{JT}, $^2B_{2g}$	0.13	0.13	0.17
	R_{JT}, $^2B_{3g}$	0.15	0.14	0.17
MnPc	E_{JT}, $^4B_{2g}$	137	178	152
	E_{JT}, $^4B_{3g}$	13	25	27
	E_{JT} (IDP), $^4B_{2g}$	142	181	178
	E_{JT} (IDP), $^4B_{3g}$	20	31	34
	Δ	124	153	125
	R_{JT}, $^4B_{2g}$	0.12	0.10	0.13
	R_{JT}, $^4B_{3g}$	0.21	0.17	0.17

View Article Online
DOI: 10.1039/C6CP03859J

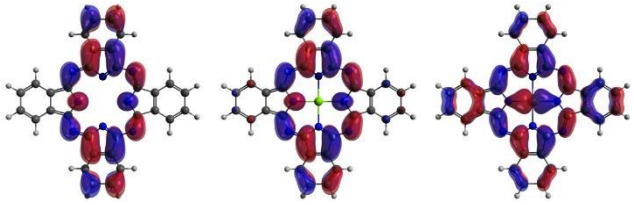

Figure 4. Schematic representation of one component of the doubly degenerate SOMOs in Pc^{3-}, $MgPc^{-}$ and MnPc.

The doubly degenerate SOMOs (D_{4h} point group), in the case of Pc^{3-} and $MgPc^{-}$ are localized on the phthalocyanine ring, Figure 4. Contrary to the situation of Pc^{3-} and $MgPc^{-}$, in the case of MnPc, the delocalization of MOs occurs over the whole molecule, Figure 4. The participation of the Mn^{II} 3d orbitals is not negligible, and at first glance, using MO analysis we can conclude that the Mn^{II} takes an important role in the JT distortion, although the quantitative picture remains secluded.

In order to clarify the origin of the JT distortion and determine whether the coordinated metal ion is the source of symmetry breaking, EDA was carried out for the HS and LS minimum structures of $MgPc^{-}$ and MnPc. First, the investigated complexes were separated into two fragments which could, in a chemical way, be responsible for the JT phenomenon. The first fragment in both, $MgPc^{-}$ and MnPc, is the divalent metal ion. While Mg^{II} is a closed-shell system, Mn^{II} is an open-shell system which could be the main reason and the source of the JT distortion in MnPc. The second fragment is Pc^{3-} for $MgPc^{-}$ and Pc^{2-} for MnPc. All the energy components for MnPc and $MgPc^{-}$ in the HS and LS configurations from EDA are given in the Supplementary information, Table S1 and Table S2.

The bonding analysis is summarized in Table 3, containing the leading components of E_{JT} from the EDA analysis, given as the relative energies between the HS and LS configurations. Relative preparation energy, ΔE_{prep} is positive in the case of MnPc, stressing that closed-shell Pc^{2-} opposes the distortion, in contrast to the case of $MgPc^{-}$. In both cases, relative interaction energy, ΔE_{int}, shows the stabilizing effect. The stabilization of E_{int} is more pronounced in the case of MnPc. Relative Pauli repulsion, ΔE_{Pauli}, is opposing the distortion in the case of MnPc, while it shows only minor effect in $MgPc^{-}$. ΔE_{elstat} is more stabilizing $MgPc^{-}$. The relative orbital interaction energy, ΔE_{orbint}, has substantial stabilizing effect in the case of MnPc, because of the overlap between Mn^{II} 3d orbitals and suitable ligand orbitals, Figure 4. ΔE_{orbint} has negligible destabilizing effect in the case of $MgPc^{-}$. In summary, the JT distortion in MnPc arises because of stabilizing orbital interactions, while E_{prep} and E_{Pauli} are opposing the distortion. In $MgPc^{-}$ the JT stabilization is due to the lowering of E_{prep} and E_{elstat}. The EDA analysis is not affected by the choice of DFA employed, Table 3. Small numerical variations arise mainly because of different geometries used in the calculations, as seen when EDA is performed with OPBE on LDA optimized geometries, Table 3.

Table 3. EDA analysis of MnPc and $MgPc^{-}$ in the HS and LS configurations with LDA and OPBE; relative energies between HS and LS structures are given in cm^{-1}.

	LDA	OPBE	OPBE/LDA*
	MnPc		
$-E_{JT}$	-136	-178	-169
ΔE_{prep}	176	103	181
ΔE_{int}	-312	-281	-350
ΔE_{Pauli}	155	39	144
ΔE_{elstat}	-156	-60	-143
ΔE_{orbint}	-311	-260	-351
	$MgPc^{-}$		
$-E_{JT}$	-400	-421	-408
ΔE_{prep}	-296	-282	-300
ΔE_{int}	-104	-139	-108
ΔE_{Pauli}	73	-8	78
ΔE_{elstat}	-182	-165	-190
ΔE_{orbint}	5	34	5

*OPBE single point on LDA geometries

The distortion from the HS nuclear arrangement, due to the JT effect, towards the LS energy minimum conformation is a displacement on the 3N-6 potential energy surface. In the realistic situations, several JT active modes are responsible for the distortion, and it is not possible to know a priori the individual role of different normal modes in the observed JT induced properties. These molecules are, thus, typical examples of the multimode JT problem. In order to ensure further insight and determine the linear vibronic coupling constants in Pc^{3-}, $MgPc^{-}$ and MnPc, the forces at the HS point were calculated toward the distortion to the LS structures, Table 4. An analysis of the multimode JT distortion shows that, out of 28 totally symmetric normal modes in the LS minimum conformation, in the case of Pc^{3-} 10 normal modes describe the distortion, Table 4. In the case of $MgPc^{-}$ and MnPc, out of 28 a_g modes, 11 vibrations are sufficient to completely characterize the distortion, Table 4. These normal modes contribute the most to the JT distortion (R_{JT}), and to the total force at the HS point.

In the case of Pc^{3-} the distortion starts with the normal mode of 1556 cm^{-1}, localized in C′-N″ bonds, Table 4 and Figures 3, 5 and 6. The vibrations of 1449 cm^{-1} (mainly localized in benzene rings of Pc^{3-}, Figure 3 and Figure 6) and 720 cm^{-1} (C′-N′-C′ bending where the opposite ones are in the same phase, Figure 3 and Figure 6) also play a role in the stabilization of the molecule, Table 4 and Figure 5. The contributions of these three normal modes to the total force decrease rapidly along the IDP path. Although the lowest frequency mode of 118 cm^{-1} does not have important contribution to the total force, it contributes the most to the overall distortion, Table 4 and Figure 5. In the second region of the IDP, this soft mode, N′N′ asymmetric stretch (Figure 3 and Figure 6), leads molecule toward the global minimum, playing the main role concerning the JT radius.

Table 4. Analysis of the multimode JT effect in Pc^{3-}, $MgPc^{-}$ and MnPc at the D_{4h} nuclear configuration: the JT radii (r_{JT},i, (amu)$^{1/2}$Å), contribution of the most relevant D_{4h} normal modes to the distortion (c_i), and the forces (linear vibronic coupling constants, F_i^{HS}, cm^{-1}/ Å) of the most relevant D_{4h} normal modes. Total force along all JT active b_{1g} modes is 19638 cm^{-1}/Å, 25297 cm^{-1}/Å and 13115 cm^{-1}/Å for Pc^{3-}, $MgPc^{-}$ and MnPc, respectively. The total r_{JT} and F^{HS} are vector sum.

Freq., cm^{-1}	r_{JT},i, (amu)$^{1/2}$Å	c_i	F_i^{HS}, cm^{-1}/Å
Pc^{3-}, $D_{4h}\rightarrow D_{2h}$			
118	0.3121	0.8637	218
531	0.0308	0.0084	820
720	0.0769	0.0525	4641
765	0.0202	0.0036	1412
1089	0.0290	0.0075	2957
1166	0.0110	0.0011	1174
1271	0.0469	0.0196	7783
1449	0.0330	0.0097	7272
1556	0.0601	0.0320	15301
1574	0.0054	0.0003	1211
Total	0.3355	0.9984	19581
$MgPc^{-}$, $D_{4h}\rightarrow D_{2h}$			
179	0.0216	0.0269	209
560	0.0179	0.0184	391
758	0.0696	0.2793	4917
796	0.0339	0.0662	2462
1116	0.0285	0.0468	3179
1200	0.0257	0.0382	3562
1327	0.0200	0.0230	3353
1410	0.0110	0.0070	2428
1454	0.0405	0.0943	8927
1592	0.0630	0.2286	16757
1602	0.0532	0.1630	14415
Total	0.1312	0.9917	25271
MnPc, $D_{4h}\rightarrow D_{2h}$			
199	0.0839	0.4653	341
568	0.0249	0.0409	844
760	0.0580	0.2226	3932
805	0.0252	0.0420	1869
1126	0.0246	0.0400	3008
1194	0.0276	0.0502	4228
1331	0.0022	0.0003	654
1420	0.0209	0.0288	4464
1458	0.0285	0.0536	6238
1605	0.0210	0.0290	5752
1634	0.0197	0.0257	5716
Total	0.1229	0.9984	13105

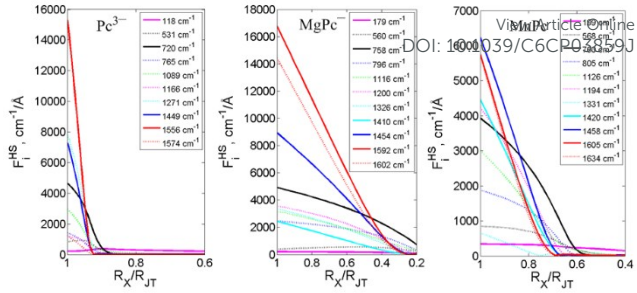

Figure 5. IDP analysis of the $D_{4h}\rightarrow D_{2h}$ multimode JT distortion in Pc^{3-}, $MgPc^{-}$ and MnPc, respectively. Changes of the forces along the most important D_{4h} normal modes.

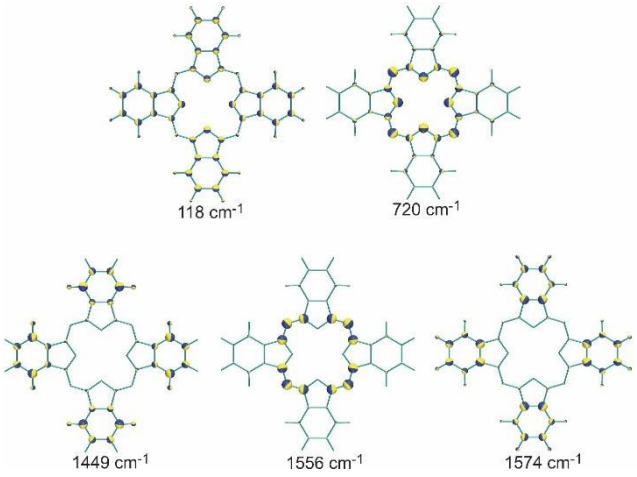

Figure 6. Schematic representation of the most important normal modes in Pc^{3-}. The size of vibrational motion on a nucleus is represented as sphere with the radius depending on the magnitude of the motion. The different colors indicate the direction of the motion.

Although coordination of Pc^{3-} to the magnesium divalent ion does not influence the doubly degenerate SOMO, Figure 4, the JT stabilization energy and the driving force are larger than in the case of Pc^{3-}, while the distortion is almost twice smaller, Tables 2 and 4. The reason behind this is in the significant participation of the harder modes in the JT distortion. However, the coordination to the metal ion makes the molecule more rigid, and thus producing smaller R_{JT}.

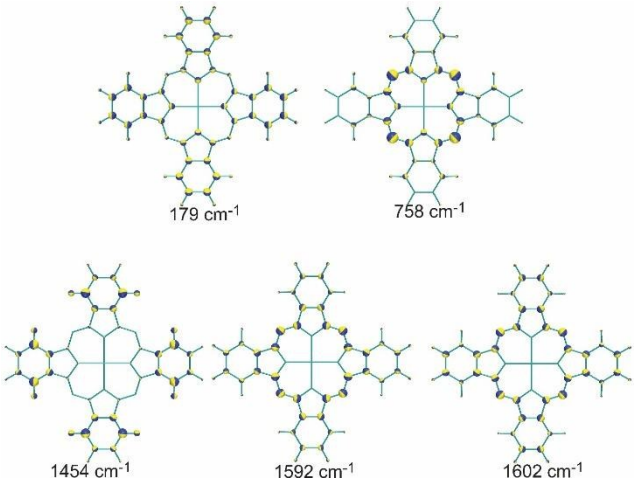

Figure 7. Schematic representation of the most important normal modes in $MgPc^-$. The size of vibrational motion on a nucleus is represented as sphere with the radius depending on the magnitude of the motion. The different colors indicate the direction of the motion.

The vibrations of 1602 and 1592 cm^{-1} correspond to the normal modes localized in the C′-N″ bonds and in benzene rings, Figures 3, 5 and 7. These two modes have the largest linear vibronic coupling constants, Table 4 and Figure 5, although the contribution of vibration of 1454 cm^{-1} localized in benzene rings, Figure 7, is non-negligible, Table 4 and Figure 5. It is interesting to notice that in contrast to the potential energy surface of Pc^{3-}, the IDP analysis did not find the softest mode of 179 cm^{-1} to contribute significantly to the JT distortion, Table 4 and Figure 5. In this case, 11 normal modes play a role in the overall distortion, while the most dominant ones are vibrations of 1602, 1592, 1454 and 758 cm^{-1}, Table 4 and Figure 5. The vibration of 758 cm^{-1} corroborates the normal mode of 720 cm^{-1} in Pc^{3-}, Figures 6 and 7.

In order to make a comparison we refer to the work of Tóbik et al.,[72] where the linear vibronic coupling constants of all the JT active modes are determined, using neutral D_{4h} MgPc geometry, as the starting point. The contribution of the b_{1g} modes to the driving force is overall in a good agreement with the previously reported values,[72] Figure 8. The only difference is in the contribution of the totally symmetric normal modes distortion. Within the IDP model, the AOC geometry of $MgPc^-$ is used. The neutral MgPc and charged $MgPc^-$ obtained by AOC type calculations have different electronic structures, and different geometries, rationalizing the discrepancy. However, if we take the geometry of the neutral MgPc as the HS structure, the values are in agreement with Tóbik et al.,[72] Figure 8, giving us the confidence in the obtained results, and showing the importance of the choice of HS geometry.

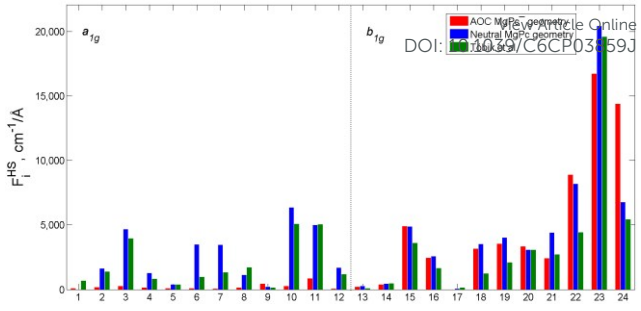

Figure 8. Comparison of the contributions to the F^{HS} of different D_{4h} normal modes in $MgPc^-$ for different D_{4h} geometries (from AOC geometry optimization of $MgPc^-$ and from neutral MgPc) with those of Tóbik et al.[72]

On the potential energy surface of MnPc, the modes of 1634, 1605 and 1458 cm^{-1} afford the largest coupling constants, and hence stabilize the molecule, Table 4 and Figures 5 and 9, although the contribution of other b_{1g} vibrations cannot be neglected since the SOMO is delocalized over the whole system (Figure 4). As a consequence, and contrary to the previously investigated species, the initial force is obtained as a superposition of more normal modes, with almost the same contribution, Table 4 and Figure 5. Soft mode of 199 cm^{-1} (Figure 9), corroborating the soft modes of 118 and 179 cm^{-1} in Pc^{3-} and $MgPc^-$, respectively (Figures 6 and 7) becomes more important in the second region, allowing relaxation, and the potential energy surface is more flat.

To summarize, IDP model successfully explained which normal modes have the most important role in the stabilization of the systems and the overall distortion. In the case of Pc^{3-} and $MgPc^-$, hard modes are responsible for the stabilization.

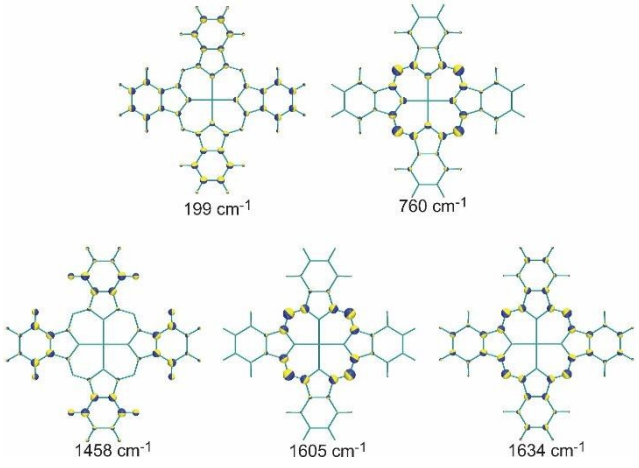

Figure 9. Schematic representation of the most important normal modes in MnPc. The size of vibrational motion on a nucleus is represented as sphere with the radius depending on the magnitude of the motion. The different colors indicate the direction of the motion.

The important difference between the multimode problems in these two molecules is that the $MgPc^-$ is not relaxed toward the global minimum structure by the softest frequency mode. Because SOMO in MnPc is delocalized over the entire molecule, it is not surprising that eleven b_{1g} normal modes in the D_{4h} nuclear configuration are almost equally important to accurately describe the relaxation of the system. There are several normal modes relevant for the stabilization, which is in contrast to the situation in Pc^{3-} and $MgPc^-$.

Conclusion

The discovery of the JT effect has become a source of inspiration for many researchers, not only as an adoption of new cognitions, but it affects many fundamental properties of molecules. In the framework of vibronic coupling theory it is possible to find rationalizations of different molecular phenomena. Since the electron doping of various metallophthalocyanines produces conductors from initial insulators, and also opens the road to the coupling of electronic states and nuclear motions, the proper determination of the JT distortion is an important prerequisite for the analysis of various properties of complex systems. Our calculations revealed that among different possible intermediate spin states, ^4E_g is the ground state in MnPc, irrespective of level of theory employed, giving the rise to the vibronic coupling.

In order to understand the origin of the JT distortion, EDA analysis in Pc^{3-}, $MgPc^-$ and MnPc is presented. Considering MnPc, leading stabilizing contributions are based on the electron density of the Mn^{II} ion, in contrast to the $MgPc^-$. It is clear that the central metal ion presents the trigger for the JT distortion to occur over the whole system. The crucial effect in the case of $MgPc^-$ is the preparation energy, acting in a stabilizing way. Since the preparation energy is completely located on the phthalocyanine ligand, the JT distortion occurs in Pc^{3-} core. To complete understanding of the JT phenomena in these similar systems, IDP model for the analysis of the multimode JT effect is successfully employed. The change of contribution of different vibrations to the JT distortion is obtained by expressing the distortion along the minimal energy path from HS to LS minimum structures. In the case of Pc^{3-} and $MgPc^-$ only hard modes take the role in the stabilization. However, careful inspection revealed that softer modes become equally important along with the hard vibrations for the accurate description of the MnPc stabilization. It is important to highlight that obtained results indicate that the JT distortion is highly influenced by the coordination of phthalocyanine to the Mn^{II} ion, while $MgPc^-$ complex ion possesses mainly ligand-based instability.

Different type of distortions and different nature of the symmetry breaking arise in these similar systems since different normal modes are responsible for the JT effect. This is of great importance, since neglecting nuclear displacements caused by an electronic structure would lead to the lack of explanation of many physical and chemical phenomena. This is certainly significant for the rational design of new phthalocyanine materials with desired properties.

View Article Online
DOI: 10.1039/C6CP03859J

Acknowledgments

This work was financially supported by the Serbian Ministry of Education and Science.

References

(1) Roth, S.; Blumentritt, S.; Burghard, M.; Cammi, E.; Carroll, D.; Curran, S.; Düsberg, G.; Liu, K.; Muster, J.; Philipp, G.; Rabenau, T. *Synthetic Metals* **1998**, *94*, 105.

(2) Jun, T. *Japanese Journal of Applied Physics* **1995**, *34*, 3864.

(3) Zhou, R.; Josse, F.; Göpel, W.; Öztürk, Z. Z.; Bekaroğlu, Ö. *Applied Organometallic Chemistry* **1996**, *10*, 557.

(4) Braun, A.; Tcherniac, J. *Berichte der deutschen chemischen Gesellschaft* **1907**, *40*, 2709.

(5) Leznoff, C. C.; Lever, A. B. P. *Phthalocyanines: Properties and Applications*; VCH: New York, 1989-1996; Vol. 1-4.

(6) Gregory, P. *Journal of Porphyrins and Phthalocyanines* **2000**, *04*, 432.

(7) Orti, E.; Bredas, J. L. *Journal of the American Chemical Society* **1992**, *114*, 8669.

(8) Craciun, M. F.; Rogge, S.; den Boer, M. J. L.; Margadonna, S.; Prassides, K.; Iwasa, Y.; Morpurgo, A. F. *Advanced Materials* **2006**, *18*, 320.

(9) Craciun, M. F.; Rogge, S.; Morpurgo, A. F. *Journal of the American Chemical Society* **2005**, *127*, 12210.

(10) Fu, Y.-S.; Xue, Q.-K.; Wiesendanger, R. *Physical Review Letters* **2012**, *108*, 087203.

(11) Liu, L.; Yang, K.; Jiang, Y.; Song, B.; Xiao, W.; Li, L.; Zhou, H.; Wang, Y.; Du, S.; Ouyang, M.; Hofer, W. A.; Castro Neto, A. H.; Gao, H.-J. *Scientific Reports* **2013**, *3*, 1210.

(12) Fu, Y.-S.; Ji, S.-H.; Chen, X.; Ma, X.-C.; Wu, R.; Wang, C.-C.; Duan, W.-H.; Qiu, X.-H.; Sun, B.; Zhang, P.; Jia, J.-F.; Xue, Q.-K. *Physical Review Letters* **2007**, *99*, 256601.

(13) Bauer, J.; Pascual, J. I.; Franke, K. J. *Physical Review B* **2013**, *87*, 075125.

(14) Stróżecka, A.; Soriano, M.; Pascual, J. I.; Palacios, J. J. *Physical Review Letters* **2012**, *109*, 147202.

(15) Wende, H.; Bernien, M.; Luo, J.; Sorg, C.; Ponpandian, N.; Kurde, J.; Miguel, J.; Piantek, M.; Xu, X.; Eckhold, P.; Kuch, W.; Baberschke, K.; Panchmatia, P. M.; Sanyal, B.; Oppeneer, P. M.; Eriksson, O. *Nat Mater* **2007**, *6*, 516.

(16) Heutz, S.; Mitra, C.; Wu, W.; Fisher, A. J.; Kerridge, A.; Stoneham, M.; Harker, A. H.; Gardener, J.; Tseng, H. H.; Jones, T. S.; Renner, C.; Aeppli, G. *Advanced Materials* **2007**, *19*, 3618.

(17) Lehmann, J.; Gaita-Arino, A.; Coronado, E.; Loss, D. *Journal of Materials Chemistry* **2009**, *19*, 1672.

(18) Clemente-Juan, J. M.; Coronado, E.; Gaita-Arino, A. *Chemical Society Reviews* **2012**, *41*, 7464.

(19) Kobayashi, N.; Leznoff, C. C. *Journal of Porphyrins and Phthalocyanines* **2004**, *08*, 1015.

(20) Brumboiu, I. E.; Haldar, S.; Lüder, J.; Eriksson, O.; Herper, H. C.; Brena, B.; Sanyal, B. *Journal of Chemical Theory and Computation* **2016**.

(21) Kroll, T.; Kraus, R.; Schönfelder, R.; Aristov, V. Y.; Molodtsova, O. V.; Hoffmann, P.; Knupfer, M. *The Journal of Chemical Physics* **2012**, *137*, 054306.

(22) Brumboiu, I. E.; Totani, R.; de Simone, M.; Coreno, M.; Grazioli, C.; Lozzi, L.; Herper, H. C.; Sanyal, B.; Eriksson, O.; Puglia, C.; Brena, B. *The Journal of Physical Chemistry A* **2014**, *118*, 927.

(23) Williamson, B. E.; VanCott, T. C.; Boyle, M. E.; Misener, G. C.; Stillman, M. J.; Schatz, P. N. *Journal of the American Chemical Society* **1992**, *114*, 2412.

(24) Kataoka, T.; Sakamoto, Y.; Yamazaki, Y.; Singh, V. R.; Fujimori, A.; Takeda, Y.; Ohkochi, T.; Fujimori, S. I.; Okane, T.; Saitoh, Y.; Yamagami, H.; Tanaka, A. *Solid State Communications* **2012**, *152*, 806.

(25) Marom, N.; Kronik, L. *Applied Physics A* **2009**, *95*, 165.

(26) Petraki, F.; Peisert, H.; Hoffmann, P.; Uihlein, J.; Knupfer, M.; Chassé, T. *The Journal of Physical Chemistry C* **2012**, *116*, 5121.

(27) Mitra, S.; Gregson, A. K.; Hatfield, W. E.; Weller, R. R. *Inorganic Chemistry* **1983**, *22*, 1729.

(28) Jahn, H. A.; Teller, E. *Proceedings of the Royal Society of London A* **1937**, *161*, 220.

(29) Bersuker, I. *The Jahn-Teller Effect*; Cambridge University Press, 2006.

(30) Bruyndonckx, R.; Daul, C.; Manoharan, P. T.; Deiss, E. *Inorganic Chemistry* **1997**, *36*, 4251.

(31) Zlatar, M.; Schläpfer, C.-W.; Daul, C. In *The Jahn-Teller Effect*; Köppel, H., Yarkony, D. R., Barentzen, H., Eds.; Springer Berlin Heidelberg: 2009; Vol. 97, p 131.

(32) Gruden-Pavlović, M.; García-Fernández, P.; Andjelković, L.; Daul, C.; Zlatar, M. *The Journal of Physical Chemistry A* **2011**, *115*, 10801.

(33) Ramanantoanina, H.; Zlatar, M.; Garcia-Fernandez, P.; Daul, C.; Gruden-Pavlovic, M. *Physical Chemistry Chemical Physics* **2013**, *15*, 1252.

(34) Andjelković, L.; Gruden-Pavlović, M.; Daul, C.; Zlatar, M. *International Journal of Quantum Chemistry* **2013**, *113*, 859.

(35) Ramanantoanina, H.; Gruden-Pavlovic, M.; Zlatar, M.; Daul, C. *International Journal of Quantum Chemistry* **2013**, *113*, 802.

(36) Zlatar, M.; Schläpfer, C.-W.; Fowe, E. P.; Daul, C. A. *Pure and Applied Chemistry* **2009**, *81*, 1397.

(37) Bickelhaupt, F. M.; Baerends, E. J. In *Reviews in Computational Chemistry*; John Wiley & Sons, Inc.: 2007, p 1.

(38) Swart, M. *Inorganica Chimica Acta* **2007**, *360*, 179.

(39) Andjelković, L.; Gruden-Pavlović, M.; Zlatar, M. *Chemical Physics* **2015**, *460*, 64.

(40) Zlatar, M.; Gruden-Pavlović, M.; Schläpfer, C.-W.; Daul, C. *Journal of Molecular Structure: THEOCHEM* **2010**, *954*, 86.

(41) Baerends, E. J.; Autschbach, J.; Bérces, A.; Berger, J. A.; Bickelhaupt, F. M.; Bo, C.; de Boeij, P. L.; Boerrigter, P. M.; Cavallo, L.; Chong, D. P.; Deng, L.; Dickson, R. M.; Ellis, D. E.; van Faassen, M.; Fan, L.; Fischer, T. H.; Fonseca Guerra, C.; van Gisbergen, S. J. A.; Groeneveld, J. A.; Gritsenko, O. V.; Grüning, M.; Harris, F. E.; van den Hoek, P.; Jacob, C. R.; Jacobsen, H.; Jensen, L.; Kadantsev, E. S.; van Kessel, G.; Klooster, R.; Kootstra, F.; van Lenthe, E.; McCormack, D. A.; Michalak, A.; Neugebauer, J.; Nicu, V. P.; Osinga, V. P.; Patchkovskii, S.; Philipsen, P. H. T.; Post, D.; Pye, C. C.; Ravenek, W.; Romaniello, P.; Ros, P.; Schipper, P. R. T.; Schreckenbach, G.; Snijders, J. G.; Solà, M.; Swart, M.; Swerhone, D.; teVelde, G.; Vernooijs, P.; Versluis, L.; Visscher, L.; Visser, O.; Wang, F.; Wesolowski, T. A.; van Wezenbeek, E. M.; Wiesenekker, G.; Wolff, S. K.; Woo, T. K.; Yakovlev, A. L.; Ziegler, T.; SCM, Theoretical Chemistry, Vrije Universiteit Amsterdam: Amsterdam, The Netherlands, 2010.

(42) Guerra, C. F.; Snijders, J. G.; teVelde, G.; Baerends, E. J. *Theoretical Chemistry Accounts* **1998**, *99*, 391.

(43) te Velde, G.; Bickelhaupt, F. M.; Baerends, E. J.; Fonseca Guerra, C.; van Gisbergen, S. J. A.; Snijders, J. G.; Ziegler, T. *Journal of Computational Chemistry* **2001**, *22*, 931.

(44) Vosko, S. H.; Wilk, L.; Nusair, M. *Canadian Journal of Physics* **1980**, *58*, 1200.

(45) Swart, M.; Ehlers, A. W.; Lammertsma *, K. *Molecular Physics* **2004**, *102*, 2467.

(46) Stephens, P. J.; Devlin, F. J.; Chabalowski, C. F.; Frisch, M. J. *The Journal of Physical Chemistry* **1994**, *98*, 11623.

(47) Van Lenthe, E.; Baerends, E. J. *Journal of Computational Chemistry* **2003**, *24*, 1142.

(48) Chong, D. P.; Van Lenthe, E.; Van Gisbergen, S.; Baerends, E. J. *Journal of Computational Chemistry* **2004**, *25*, 1030.

(49) Becke, A. D. *Physical Review A* **1988**, *38*, 3098.

(50) Perdew, J. P. *Physical Review B* **1986**, *33*, 8822.

(51) Perdew, J. P. *Physical Review B* **1986**, *34*, 7406.

(52) Swart, M. *Chemical Physics Letters* **2013**, *580*, 166.

(53) Zhao, Y.; Truhlar, D. G. *The Journal of Chemical Physics* **2006**, *125*, 194101.

(54) del Campo, J. M.; Gázquez, J. L.; Trickey, S. B.; Vela, A. *The Journal of Chemical Physics* **2012**, *136*, 104108.

(55) Ernzerhof, M.; Scuseria, G. E. *The Journal of Chemical Physics* **1999**, *110*, 5029.

(56) Tao, J.; Perdew, J. P.; Staroverov, V. N.; Scuseria, G. E. *Physical Review Letters* **2003**, *91*, 146401.

(57) Franchini, M.; Philipsen, P. H. T.; Visscher, L. *Journal of Computational Chemistry* **2013**, *34*, 1819.

(58) Becke, A. D. *The Journal of Chemical Physics* **1988**, *88*, 2547.

(59) Ziegler, T.; Rauk, A. *Inorganic Chemistry* **1979**, *18*, 1558.

(60) Ziegler, T.; Rauk, A. *Inorganic Chemistry* **1979**, *18*, 1755.

(61) Kirner, J. F.; Dow, W.; Scheidt, W. R. *Inorganic Chemistry* **1976**, *15*, 1685.

(62) Kitaoka, Y.; Sakai, T.; Nakamura, K.; Akiyama, T.; Ito, T. *Journal of Applied Physics* **2013**, *113*, 17E130.

(63) Liao, M.-S.; Watts, J. D.; Huang, M.-J. *Inorganic Chemistry* **2005**, *44*, 1941.

(64) Reynolds, P. A.; Figgis, B. N. *Inorganic Chemistry* **1991**, *30*, 2294.

(65) Barraclough, C. G.; Martin, R. L.; Mitra, S.; Sherwood, R. C. *The Journal of Chemical Physics* **1970**, *53*, 1638.

(66) Granatier, J.; Dubecký, M.; Lazar, P.; Otyepka, M.; Hobza, P. *Journal of Chemical Theory and Computation* **2013**, *9*, 1461.

(67) Gruden-Pavlovic, M.; Stepanovic, S.; Peric, M.; Guell, M.; Swart, M. *Physical Chemistry Chemical Physics* **2014**, *16*, 14514.

(68) Maja, G.; Stepan, S.; Marcel, S. *Journal of the Serbian Chemical Society* **2015**, *80*, 1399.

(69) Zlatar, M.; Gruden-Pavlovic, M.; Guell, M.; Swart, M. *Physical Chemistry Chemical Physics* **2013**, *15*, 6631.

(70) Milko, P.; Iron, M. A. *Journal of Chemical Theory and Computation* **2014**, *10*, 220.

(71) Hug, W.; Fedorovsky, M. *Theoretical Chemistry Accounts* **2008**, *119* 113.

(72) Tóbik, J.; Tosatti, E. *Journal of Molecular Structure* **2007**, *838*, 112.